Inorganic Chemistry

ARTICLE

pubs.acs.org/IC

Drastic Change of the Ferromagnetic Properties of the Ternary Germanide GdTiGe through Hydrogen Insertion

Etienne Gaudin,*[,†] Samir F. Matar,[†] Rainer Pöttgen,[‡] Matthias Eul,[‡] and Bernard Chevalier[†]

[†]CNRS, Université de Bordeaux, ICMCB, 87 Avenue du Docteur Albert Schweitzer, 33608 Pessac Cedex, France

[‡]Institut für Anorganische und Analytische Chemie, Universität Münster, Corrensstrasse 30, 48149 Münster, Germany

ABSTRACT: Hydrogen absorption of the CeFeSi- and CeScSi-type forms of GdTiGe was performed. Before hydrogenation they show an antiferromagnetic transition at around 412 K and a ferromagnetic transition at 376 K, respectively. Hydrogenation of both forms leads to formation of the same hydride GdTiGeH which crystallizes with a filled CeScSi-type structure where all the $[Gd_4]$ tetrahedra are filled by hydrogen. This hydride is paramagnetic in the temperature range 4−300 K. The slightly negative value of the paramagnetic Curie temperature θ_p confirms that all ferromagnetic interactions were destroyed in the case of the CeScSi-type form. From first-principles calculations with the PAW GGA methodology, the localization of hydrogen within the $[Gd_4]$ tetrahedra was confirmed through energetic stabilization. It was also seen that the energy changes significantly with volume, indicating the itinerant (delocalized) role of the electrons in the magnetism.

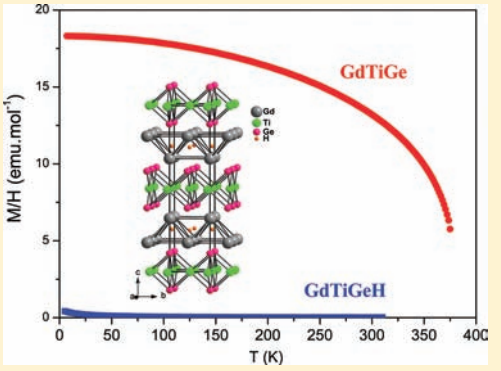

INTRODUCTION

Recently, the discovery of superconductivity properties in the family of ZrCuSiAs-type compounds[1−3] has attracted much attention. The crystal structure of these compounds derives from the tetragonal anti-PbFCl type structure (*P*4/*nmm*) and can be described by the stacking along the *c* direction of two different layers. In LaFePO,[1] for instance, one layer is made of $[P_4]$ tetrahedra filled by Fe and the other one of $[La_4]$ tetrahedra filled by O. Within both layers the tetrahedra are sharing edges. In intermetallics, many ternary compounds with the general formula *RETX* (*RE* = rare-earth, *T* = transition metal, and *X* = p metal) crystallize with the so-called tetragonal CeFeSi-type structure which indeed corresponds to the anti-PbFCl structure. In CeFeSi one layer is made of p metal tetrahedra $[Si_4]$ filled by the transition metal Fe and the other one of empty rare-earth tetrahedra $[Ce_4]$. The filling of these latter tetrahedra by hydrogen atoms during hydrogenation was realized in the past.[4−8] Many studies on these hydrides crystallizing with the ZrCuSiAs-type structure show changes in the magnetic properties through the filling of the $[RE_4]$ tetrahedra by hydrogen. For instance, transition from a heavy fermion system to antiferromagnetic ordering[6] or from an antiferromagnetic to ferromagnetic ordering[8] was observed, respectively, during hydrogenation of CeRuSi and NdCoSi.

Among *RETX* intermetallics some of them are crystallizing with the CeScSi structure, which can be easily related to the CeFeSi-type. The former structure corresponds to an ordered variant of the La_2Sb-type structure. Very recently, superconductivity below 5 K was observed for La_2Sb.[9] In this structure a layer made up of empty edge-sharing rare-earth tetrahedra $[La_4]$ is observed like in an anti-PbFCl structure. The main difference between the CeFeSi- and the CeScSi-type structures concerns the [FeSi] layer. This layer is made in the former of edge-shared $[Si_4]$ tetrahedra filled by Fe and in the latter of $[Si_4]$ square planes with Sc in the center. Few *RETX* ternary compounds crystallize with this structural type. The main series are *RE*ScSi (*RE* = Ce, Pr, Nd, Sm, Gd),[10,11] *RE*ScGe (*RE* = Ce, Pr, Nd, Sm, Gd, Tb),[10−12] *RE*TiGe (*RE* = Y, Ce, Sm, Gd, Tb),[10,13−15] and *RE*ZrSb (*RE* = Y, Gd−Tm, Lu).[16] Other intermetallic series are known with, for instance, magnesium instead of a transition metal within the series *RE*MgSn (*RE* = Y, Nd, Sm, Gd−Tm, Lu).[17,18]

The filling of the empty $[RE_4]$ tetrahedra by hydrogen, as previously realized with anti-PbFCl-type compounds (vide infra), was successfully achieved for CeScSi and CeScGe. Hydrogen insertion induces an anisotropic unit cell expansion, and this leads to a significant decrease of the antiferromagnetic ordering temperatures with an increase of the Kondo interactions.[19]

The case of the *RE*TiGe ternary germanides is interesting since both structural types, CeFeSi and CeScSi, can be stabilized. Recently, we completed a structural study of this series with the synthesis of the new CeScSi-type polymorph of CeTiGe.[13] In this series, the CeFeSi- and CeScSi-type forms of GdTiGe show an antiferromagnetic transition at around 412 K and a ferromagnetic transition at 376 K.[14,20] In our search of new compounds with a high magnetocaloric effect (MCE) for magnetic refrigeration, the existence of a ferromagnetic transition in the vicinity of room temperature is of great interest.[21,22] To tune the Curie temperature, chemical substitution or insertion of light elements is the usual way. For instance, in the promising class of intermetallics

Received: July 22, 2011
Published: October 11, 2011

Table 1. Lattice Parameters (XRD powder data) of GdTiGe and GdTiGeH

sample	composition	structure-type	a (Å)	c (Å)	V (Å^3)	ref
A	GdTiGe	CeScSi	4.0645(5)	15.448(2)	255.20(6)	*a*
B	$Gd_{0.95}TiGe_{0.95}$	CeScSi	4.0669(2)	15.4603(6)	255.70(2)	*a*
		CeFeSi	4.0666(2)	7.7295(5)	127.82(1)	*a*
hydrogenated A	GdTiGeH	filled CeScSi	3.9848(8)	16.407(3)	260.5(1)	*a*
hydrogenated B	GdTiGeH	filled CeScSi	3.9801(3)	16.428(2)	260.24(4)	*a*
literature	GdTiGe	CeScSi	4.060(1)	15.412(1)	254.05	14
		CeFeSi	4.060(1)	7.708(1)	127.06	14
	$GdTi_{0.9}Ge$	CeScSi	4.071(1)	15.422(1)	255.59	14
	GdTiGe	CeScSi	4.065(1)	15.454(1)	255.37	25
		CeFeSi	4.069(1)	7.725(1)	127.90	25
	GdTiGeH	"filled CeScSi"	3.94	16.31	253.04	25

[a] This work.

$La(Fe_xSi_{1-x})_{13}$ with huge MCE, hydrogenation allows one to change T_C according to the hydrogen content.[23,24] Then, we decided to undertake hydrogenation of both forms of GdTiGe, especially the ferromagnetic one, to see if it is possible to tune their magnetic properties through hydrogen insertion.

A previous study of the mechanical hydrogenation of GdTiGe showed that around 4 hydrogen atoms per formula unit (4 H/f.u.) were absorbed for the CeScSi-type structure with a sharp decrease in magnetization, whereas the CeFeSi one remains passive.[25] From our expertise in the hydrogenation of the CeFeSi-type compounds it was surprising that no hydrogen absorption was observed for this latter form of GdTiGe. Moreover, in both structural types one would expect absorption of only one H/f.u. with the filling of all $[Gd_4]$ tetrahedra. A new study of hydrogen absorption of both forms of GdTiGe was then performed. It will be shown in this paper how hydrogenation induces a drastic change of the magnetic properties of GdTiGe and that both forms absorb 1 H/f.u. For both forms the same hydride GdTiGeH was obtained, and its crystal structure, magnetic, and electrical properties will be presented. Band structure calculations were also performed in order to understand the loss of the magnetic ordering through hydrogenation.

EXPERIMENTAL SECTION

Synthesis and Hydrogenation. Starting materials for preparation of the two GdTiGe samples were pieces of gadolinium, titanium, and germanium, all with stated purities better than 99.9%. They were placed in 1:1:1 and 0.975:1.05:0.975 atomic ratios for samples A and B, respectively, in an induction furnace. Melting of these mixtures in a high-purity argon atmosphere was made three times to ensure homogeneity, and ingots with bright metallic luster were obtained. With this procedure, the total weight loss (less than 0.2%) was negligible. Then, parts of the ingots of samples A and B were heated under vacuum at 523 K for 12 h and then exposed to 4 MPa of hydrogen gas at the same temperature. The amount of absorbed H was determined volumetrically by monitoring pressure changes in a calibrated volume.[26] The amount of H atom inserted for both samples is 1.0(1) per GdTiGe formula unit. The formed hydrides are stable in air.

X-ray Powder Diffraction. The GdTiGe and GdTiGeH samples were characterized at room temperature through a Philips 1050-diffractometer (Cu Kα radiation). Only the CeScSi-type form was observed for sample A and both forms for sample B. The tetragonal lattice parameters were obtained through a least-squares routine (Table1). To determine the respective amount of the CeFeSi- and CeScSi-type forms in sample B, XRD data with higher accuracy were collected with a Philips X-Pert diffractometer operating at room temperature and using Cu Kα_1 radiation (λ = 1.54051 Å). The powder diffraction pattern was scanned over the 2θ angular range 10.012−119.988° with a step size of 0.008°. Rietveld refinement was performed using the Jana2006 program package.[27] The background was estimated by a Legendre function with 12 parameters, and the peak shapes were described by a pseudo-Vogt function for both forms. A correction for roughness (Bragg−Brentano geometry) was also introduced. It was difficult to perfectly fit the diffraction pattern because of the strong preferred orientation observed for the CeScSi form. Nevertheless, the relative phase amounts in mass were estimated equal to 72(1)% and 28(1)% for the CeFeSi and CeScSi forms, respectively.

Table 2. Crystal Data and Structure Refinement[a] for GdTiGeH

compound	GdTiGeH
cell setting, space group	tetragonal, $I4/mmm$
a, c (Å)	3.981(4), 16.378(4)
Z, D_x (g cm^{-3})	4, 7.10
radiation type, μ (mm^{-1})	Mo Kα, 40.1
diffractometer	Nonius Kappa CCD
abs corr, shape	Gaussian, block
T_{min}, T_{max}	0.264, 0.517
no. of measd reflns	863
no. of independent reflns, R_{int}	165, 0.065
no. of observed reflns ($I > 2\sigma(I)$)	149
$2\theta_{max}$ (deg)	64.0
refinement on	F^2
$R(F^2 > 2\sigma(F^2))$, $wR(F^2)$, S	0.0241, 0.0595, 1.19
no. of reflns, refined params	165, 10
Weighting scheme	$w = 1/(\sigma^2(I) + 0.0009I^2)$
$\Delta\rho_{max}$, $\Delta\rho_{min}$ (e Å^{-3})	1.25, −1.03

[a] Computer program: Jana2006.[27]

X-ray Single-Crystal Diffraction. Refinement of the crystal structure of GdTiGeH was performed using single-crystal X-ray diffraction data, collected with an Enraf-Nonius Kappa charge-coupled device (CCD) area-detector diffractometer (Mo Kα radiation). On the basis of their shape, several single crystals were selected in the hydrogenated sample A. After the cell orientation-matrix searching procedure, data collection was performed at room temperature on the single crystal with the best quality of the intensity spots. A Gaussian-type absorption correction was applied during data processing using the shape determined with the video microscope of

dx.doi.org/10.1021/ic201579r |*Inorg. Chem.* 2011, 50, 11046–11054

the diffractometer. Data processing and all refinements were performed with the Jana2006 program package (Table 2).[27] The structure was refined with space group *I4/mmm* starting from the position of the pristine compound GdTiGe.[28] The hydrogen position was not introduced. At the end of the refinement with anisotropic displacement parameters the reliability factors R/R_w were equal to 2.41/5.95% for GdTiGeH, with residual electron densities in the range [−1.03, +1.25 e Å^{-3}]. Details of data collections, structure refinements, and the atomic parameters are listed in Tables 2 and 3. Further details may be obtained from Fachinformationszentrum Karlsruhe, D-76344 Eggenstein-Leopoldshafen (Germany) by quoting the Registry No's. CSD-423365.

Physical Property Measurements. For electrical resistivity measurements, the hydride sample B was compacted at room temperature (compactness ≈ 80%) in order to form a pellet (diameter = 6 mm and thickness = 3 mm) and then heated for 2 days at 523 K under hydrogen pressure (4 MPa). After thermal treatment, which improves the mechanical behavior, the pellet was checked by X-ray diffraction; no structural change was evidenced. For electrical resistivity (ρ), a bar of 1.5 × 1.5 × 5 mm^3 was cut from the pellet. The measurement was carried out above 4.2 K using the standard dc four--probe method with silver paint contacts and an intensity current of 10 mA. Due to the small compactness and the presence of microcracks into this bar, the absolute value of ρ could not be determined accurately; for this reason, a normalized representation $\rho(T)/\rho(270\ K)$ was given. Magnetization measurements were performed on samples A and B before and after hydrogenation. These measurements were carried out in the temperature range of 4−375 K using a superconducting quantum interference device magnetometer (SQUID, Quantum Design) and above room temperature in the range of 300−700 K using a PPMS (Quantum Design). All measurements were performed under an applied magnetic field of 500 Oe.

Computational Details. Two computational methods were used in the framework of density functional theory (DFT).[29,30] A pseudopotential approach within the Vienna ab initio simulation package (VASP) code[31] was first called for to obtain the equation of states (EOS) for GdTiGe and its hydride with projector-augmented wave (PAW) potentials[32,33] necessary for an account of 4f(Gd) states, built within the generalized gradient approximation (GGA) scheme.[34] The calculations were converged at an energy cutoff of 300 eV for the plane-wave basis set with respect to the *k*-point integration with a starting mesh of 4 × 4 × 4 up to 8 × 8 × 8 for best convergence and relaxation to zero strains. The Brillouin-zone integrals were approximated using a special *k*-point sampling.

The all-electron calculations are based on the DFT and GGA functional.[34] They were performed using the full potential scalar-relativistic augmented spherical wave (ASW) method.[35] In this method, the wave function is expanded in atom-centered augmented spherical waves, which are Hankel functions and numerical solutions of Schrödinger's equation, respectively, outside and inside the so-called augmentation spheres. In the minimal ASW basis set, we chose the outermost shells to represent the valence states and the matrix elements were constructed using partial waves up to $l_{max} + 1 = 4$ for Gd, i.e., 4f(Gd) were considered within the basis set, $l_{max} + 1 = 3$ for Ti and Ge, and finally $l_{max} + 1 = 2$ for H. Self-consistency was achieved by a highly efficient algorithm for convergence acceleration.[36] The Brillouin zone integrations were performed using the linear tetrahedron method with up to 1088 *k* points within the irreducible wedge.[35]

The relative magnitude of the chemical bonding is obtained based on the overlap population analysis: S_{ij}, *i* and *j* being two chemical species. The crystal orbital overlap population (COOP) criterion is used.[37] For the purpose of establishing trends of chemical bonding strength, we show the integrated COOP (*i*COOP): the larger the area below the curves the larger the bonding is. In the plots positive, negative, and zero *i*COOP magnitudes indicate bonding, antibonding, and nonbonding interactions, respectively.

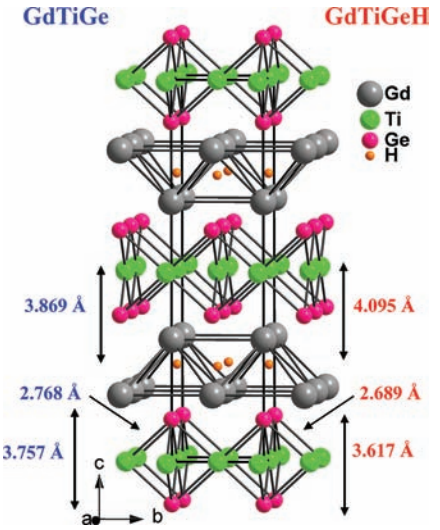

Figure 1. Crystal structure of GdTiGeH. Two-dimensional TiGe network and layers of face-shared [Gd_4] tetrahedra are emphasized. Hydrogen atoms were located in the center of the [Gd_4] tetrahedra. On the left (right) part of the figure selected distances for GdTiGe (GdTiGeH) are given.

RESULTS AND DISCUSSION

Crystal Chemistry. GdTiGe (sample A in Table 1) with the CeScSi-type structure was obtained after melting of the elements. Welter et al. obtained the same structural form after melting followed by an annealing for 4 weeks at 1273 K.[28] They classify this structural form as the low-temperature modification since they report that another study has shown that the CeFeSi-type structure can be stabilized by fast quenching.[38] However, in this reference it is stated that the compounds were annealed at 1180 K for 210 h before quenching. Thus, as previously proposed during the investigation of CeTiGe, the CeScSi-type form may correspond to a high-temperature modification.[13] It was later shown by Morozkin et al. that indeed the starting composition plays an important role for stabilization of the two different polymorphs.[14] They show that a little excess of titanium leads to stabilization of the CeFeSi-type form. This is why a different starting composition was used for the synthesis of sample B. Understanding the stabilization factors of only one of the two polymorphic forms is beyond the aim of this paper and will not be developed further.

GdTiGeH single crystals suitable for X-ray diffraction were only found in the hydrogenated sample A. The cell parameters are close to the ones determined from X-ray analysis of the two powder samples (Tables 1 and 2). On Figure 1 the structure of GdTiGeH is drawn by assuming the filling of [Gd_4] tetrahedra by hydrogen atoms. Two types of layers can be distinguished. The first one is made of hydrogen-filled [Gd_4] tetrahedra which are sharing edges and the second one of [Ge_4] squares with Ti in the centers. As mentioned in a previous paper, the main change in the atomic positions of the metallic network before and after hydrogenation is the shift of the *z* coordinate of Ge.[19] This induces a small increase of the compactness of the TiGe layer, whereas the *c* parameter significantly increases (+6.2%). As shown in Figure 1 and reported in Table 4 the Ti−Ge interatomic distances slightly decrease from 2.768 to 2.689 Å after hydrogenation and the distance Ge−Ge which corresponds to

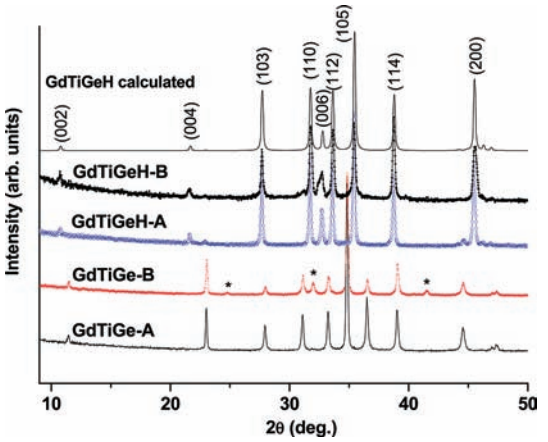

Figure 2. XRD powder pattern of the two samples of GdTiGe before and after hydrogenation measured with Cu Kα radiation at T = 293 K. For sample B of GdTiGe the asterisks indicate the peaks corresponding to the CeFeSi-type form which do not overlap with the ones of the CeScSi-type one. The upper pattern is a theoretical one calculated with the single-crystal data of GdTiGeH (Table 3).

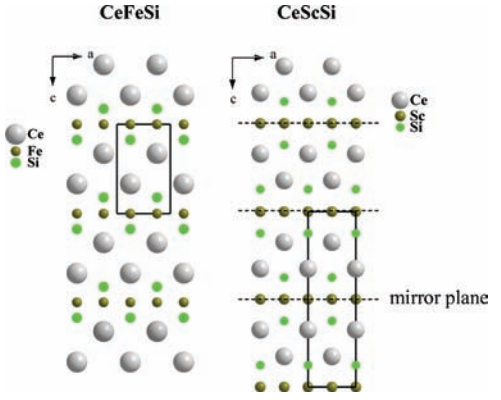

Figure 3. Projection of the structure-types CeFeSi and CeScSi along the b axis. Mirror plane for CeScSi is emphasized.

the thickness of the TiGe layer is decreasing from 3.757 to 3.617 Å. A similar behavior is observed for the Gd layer with a decrease of the Gd−Gd distances from 3.700 to 3.634 Å and from 4.067 to 3.981 Å in the (a,b) plane. These last distances correspond to the value of the a axis. The main structural effect induced through hydrogenation is a significant increase of the distance between both types of layers. This distance, which is equal to $c/4$, is going from 3.869 to 4.095 Å. From the stoichiometry in hydrogen calculated after hydrogenation (see the above Experimental Section) and by analogy with the results obtained on closely related compounds with the CeFeSi-type structure, a filling of the $[Gd_4]$ tetrahedra by hydrogen atoms is expected. This position corresponds to the Wyckoff site 4d (0, 1/2, 1/4). The Gd−H distance calculated with this ideal position is equal to 2.298 Å and very close to the one observed in GdH_2 (2.296 Å) for which H atoms are also localized in $[Gd_4]$ tetrahedra.[39] Neutron diffraction experiments on the homologous compound CeScGeH are planned to confirm the localization of the hydrogen atoms.[19]

The XRD powder patterns obtained for the samples A and B, before and after hydrogenation, are displayed in Figure 2. The sample B consists of a mixing of CeFeSi- and CeScSi-type forms

Table 3. Atomic Coordinates and Equivalent Isotropic Displacement Parameters (Å^2) for the Metal Atoms in GdTiGeH (space group $I4/mmm$, a = 3.981(4) Å and c = 16.378(4) Å)

atom	site	x	y	z	U_{eq} (Å^2)
Gd	4e	0	0	0.32015(3)	0.00632(13)
Ti	4c	0	1/2	0	0.0060(5)
Ge	4e	0	0	0.11042(7)	0.0066(2)

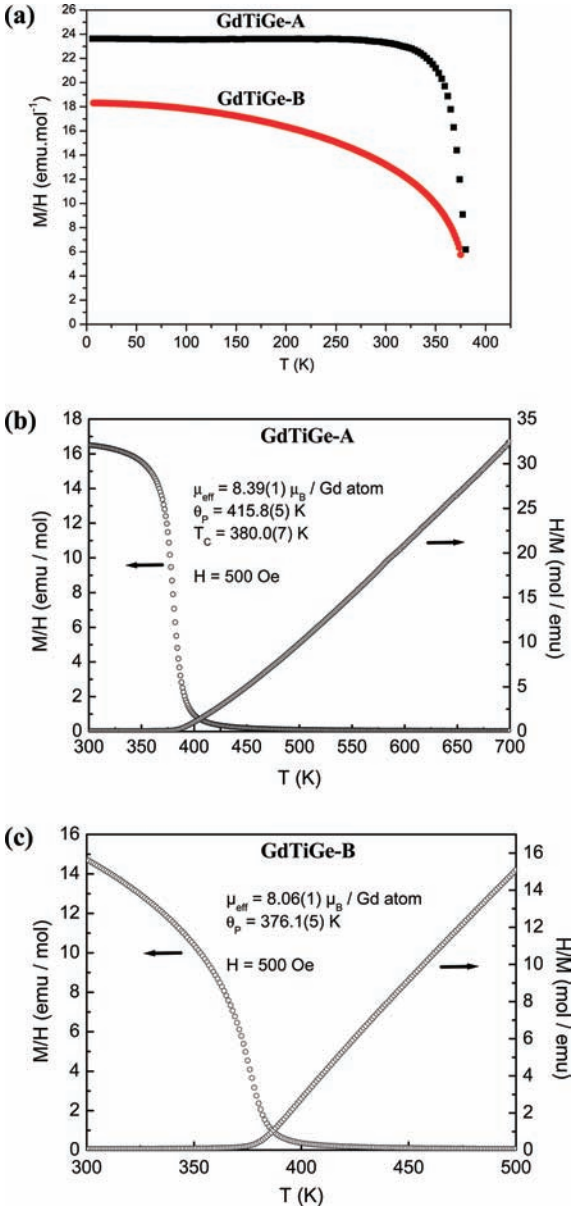

Figure 4. Temperature dependence of the magnetization M divided by the applied field H = 500 Oe and H/M for the pristine compounds GdTiGe. The temperature ranges are (a) 4−300 K for both samples, (b) 300−700 K for sample A, and (c) 300−500 K for sample B.

with a respective amount of 72(1) and 28(1) wt%. For both hydrogenated samples the same GdTiGeH phase is observed. It crystallizes with a filled CeScSi-type structure (see above) and the average cell parameters a = 3.98 and c = 16.42 Å (Table 1)

dx.doi.org/10.1021/ic201579r |Inorg. Chem. 2011, 50, 11046–11054

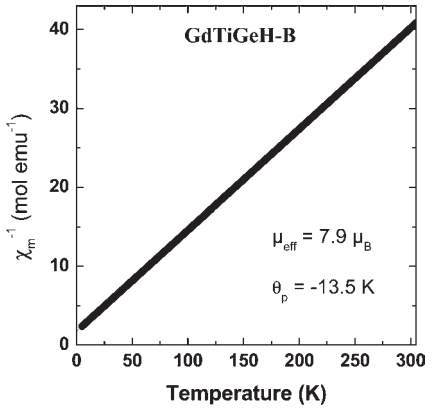

Figure 5. Temperature dependence of the reciprocal magnetic susceptibility χ_m^{-1} measured with an applied field of 30 kOe of the hydride GdTiGeH obtained through hydrogenation of sample B. Values used for the fit of the χ_m^{-1} curve made with a Curie−Weiss law are displayed.

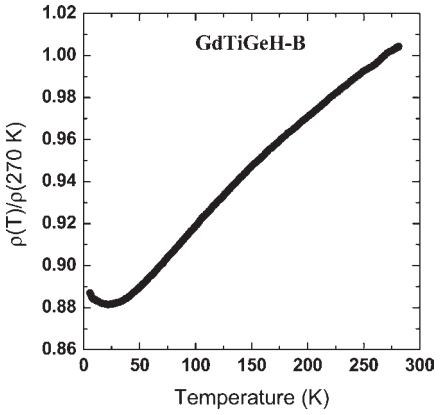

Figure 6. Temperature dependence of the normalized electrical resistivity $\rho(T)/\rho(270\ K)$ of the hydride GdTiGeH obtained through hydrogenation of sample B.

which are close to the ones determined on the single-crystal (Table 2). For the help of the discussion a diffraction pattern was calculated from the structural parameters obtained during the single-crystal investigation and this is displayed in Figure 2. It appears that when the CeFeSi-type form in sample B absorbs hydrogen a simple anisotropic evolution of the cell is not observed as previously reported for homologous compounds.[4−8] A structural change CeFeSi-type → CeScSi-type filled by H atoms takes place which induces strong structural strains. Indeed the doubling of the *c*-parameter for the CeScSi-type structure is correlated to the existence of a mirror plane located in between two [Gd_4] layers (Figure 3). This explains the strong broadening of the diffraction peaks (00*l*) which can be attributed to the existence of many stacking faults along the *c*-direction (Figure 2). It can be noticed that this broadening is very important for the reflection (006). Existence of such stacking faults may explain why no single-crystals suitable for an XRD study were found in the hydrogenated sample B. To characterize these stacking faults, transmission electron microscopy experiments are planned.

The difficulty to synthesize samples of only one polymorphic form of GdTiGe may be attributed to the very close stability of both polymorphs. The filling of the [Gd_4] tetrahedra by hydrogen may favor the stabilization of the CeScSi-type form and this is why only this polymorph is observed for GdTiGeH.

Comparison of our results with the ones obtained by Tskhadadze et al. shows several points of disagreement.[25] They claimed that they obtained $GdTiGeH_{\sim 4}$ through hydrogenation of a GdTiGe sample treated by ball milling under hydrogen. This last hydride corresponds indeed to GdTiGeH since almost the same unit cell parameters were calculated from powder XRD (a = 3.94 and c = 16.31 Å[25]). Moreover, we clearly showed that the CeFeSi-type form absorbs hydrogen in contrast to what they stated. Complete hydrogenation of our two A and B samples clearly evidenced that only a single phase GdTiGeH was obtained. The GdTiGe host structure does not provide crystal chemically suitable tetrahedral voids for more than one hydrogen atom per formula unit. The difficulty to synthesize samples of only one polymorphic form of GdTiGe may be attributed to the very close stability of both polymorphs. The filling of the [Gd_4] tetrahedra by hydrogen may favor the stabilization of the CeScSi-type form and this is why only this polymorph is observed for GdTiGeH.

Magnetic Properties. The $M/H = f(T)$ and $H/M = f(T)$ curves for the GdTiGe samples A and B are displayed in Figure 4. For sample A, the Curie temperature T_C is equal to 380(1) K. This value, which corresponds to the minimum of the derivative curve $d(M/H)/dT = f(T)$, is very close to the one reported by Tskhadadze et al. (i.e., 376 K).[25] For sample B the ferromagnetic transition is still observed because of the significant amount of the CeScSi-type phase in the sample. However, this transition is spread out over a larger temperature interval. An antiferromagnetic transition was reported at T_N = 412 K for the CeFeSi-type form and is hidden for sample B because of the presence of the ferromagnetic phase.[25] After hydrogenation the same drastic change of the magnetic properties is observed for both samples. As shown in Figure 5 the temperature dependence of the reciprocal magnetic susceptibility $\chi_m^{-1} = f(T)$ follows a Curie−Weiss law in the measured temperature range 4−300 K with a small value of the paramagnetic Curie temperature θ_p (equal to −13.5 K for hydrogenated sample B). A paramagnetic behavior is then observed in this temperature range, and the slightly negative value of θ_p confirms that all ferromagnetic interactions were destroyed. The experimental value of the effective magnetic moment 7.9 μ_B/Gd is very close to the calculated value of 7.94 μ_B/Gd for a free Gd^{3+} ion. Band structure calculations have been performed in order to try to understand how hydrogen insertion in the [Gd_4] tetrahedra may induce such a drastic effect on the magnetic properties (see below).

Electrical Properties. Figure 6 presents the temperature dependence of the reduced electrical resistivity $\rho(T)/\rho(270\ K)$ for the hydrogenated B sample. Between 270 and 30 K the resistivity decreases with temperature as in a normal metal; no anomaly occurs in this temperature range, in agreement with the absence of a magnetic transition. On the contrary, the resistivity slowly increases below 30 K, suggesting the existence of short-range magnetic order or magnetic structures with some degree of moment disorder. X-ray powder analysis of this hydride reveals a broadening of some peaks (Figure 2) due to structural disorder.

Electronic Structure Calculations. GdTiGe is ferromagnetically ordered. Upon hydrogenation (1 H per formula unit) there is an observation of a total loss of magnetic ordering. For addressing these observations from the band theoretical methodology within DFT, a problem is relevant to the way of treating the Gd 4f shell. There are two different approaches to deal with a *RE* from the middle of the series, either treating the 4f states as

dx.doi.org/10.1021/ic201579r |*Inorg. Chem.* 2011, 50, 11046–11054

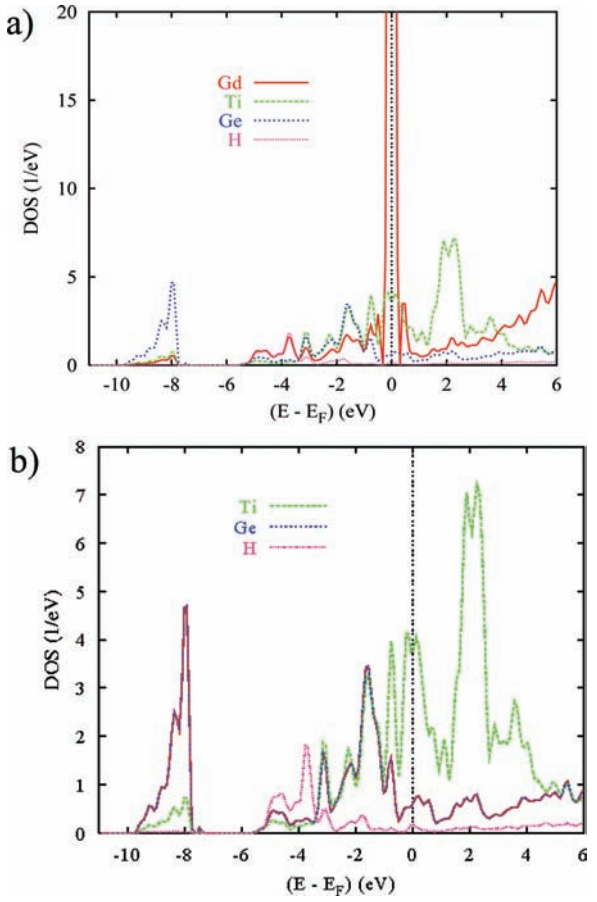

Figure 7. (a) GdTiGeH site-projected density of states in the nonmagnetic NSP configuration. (b) GdTiGeH site-projected density of states in the nonmagnetic NSP configuration discarding the Gd 4f states. Hydrogen states are seen to prevail at the lower part of the VB, i.e., −10, −8, and ∼−6 to −3.

being part of the basis set in all electrons calculations (this is successful to a certain extent for Ce-based intermetallics because Ce is an early *RE*) or by putting the 4f states deeper in energy as semicore states using either LDA+U to boost the electron-gas based correlations by an optimized U Coulomb repulsion parameter and push them further down within the valence band or appropriately built potentials such as the projector-augmented wave, PAW,[29,30] ones built with either the LDA or the gradient GGA functionals of the DFT.

We have done calculations in both approaches presented above, i.e., with the full potential ASW method for all-electron calculations and PAW-GGA with VASP code.

A. All-Electron Calculations in Spin Degenerate Configuration. An illustration of the all-electron calculations for the hydride in a nonmagnetic (NSP = nonspin-polarized) configuration is shown in Figure 7. The large DOS at the Fermi level taken as zero energy here and in the following plots (Figure 7a) is due to the Gd 4f state which is expected in as far as it is half filled, so one may expect 7 μ_B when spin-polarized (SP) calculations are done. Note also that the Ti PDOS are largely present at the Fermi level, which points to a possible polarization in the SP calculations. The DOS for the intermetallic itself look very much alike. Figure 7b shows the large contribution of Ti states (3d mainly) at E_F and the presence of H states in the lower part of the VB.

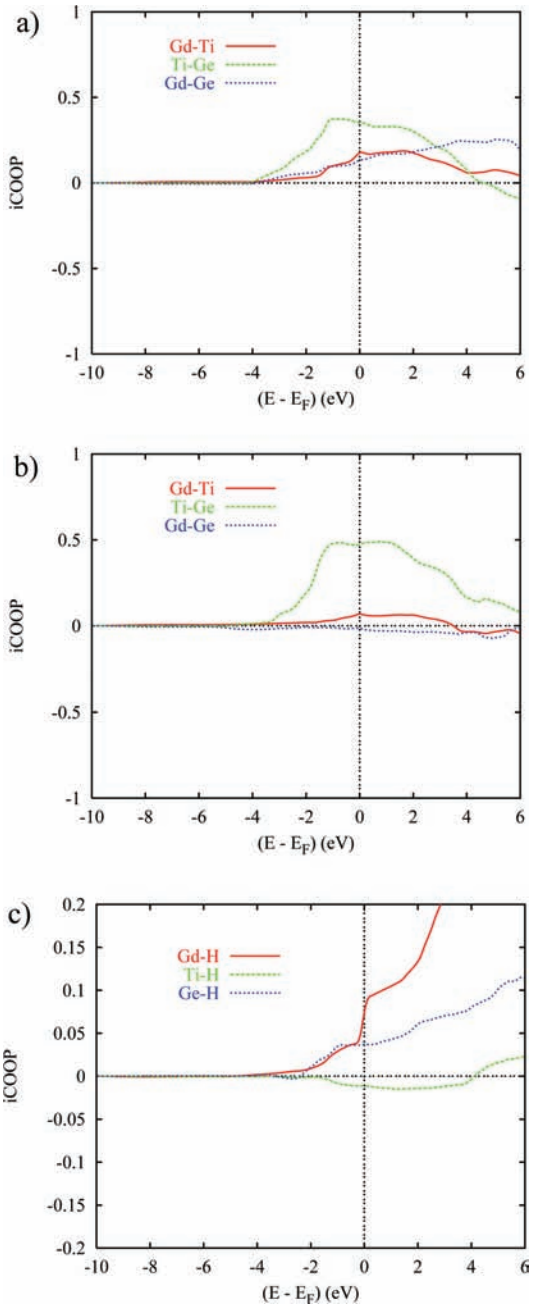

Figure 8. Chemical bonding from the COOP criterion based on the analysis of the overlap populations in GdTiGe (a) and GdTiGeH (b) and interactions of Gd, Ti, and Ge with H (c).

Looking at the chemical bonding, Figure 8 shows the pair interactions for Gd−Ti, Ti−Ge, and Gd−Ge in both GdTiGe and its hydride in Figure 8a and 8b, respectively. Figure 8c shows the 'metal'−H bonding in the hydride. While several schemes exist for the description of the relative strengths of chemical bonding (COOP, COHP, ECOV, etc.) we use here the COOP based on the overlap populations S_{ij}. With integrated COOP, *i*COOP (unitless), the larger the area below the peaks the larger the bonding is.

In GdTiGe, the prevailing interaction is for Ti−Ge with the other ones slightly smaller; on the contrary, the Ti−Ge interaction is largely enhanced in the hydrogenated compound and the

dx.doi.org/10.1021/ic201579r |*Inorg. Chem.* 2011, 50, 11046–11054

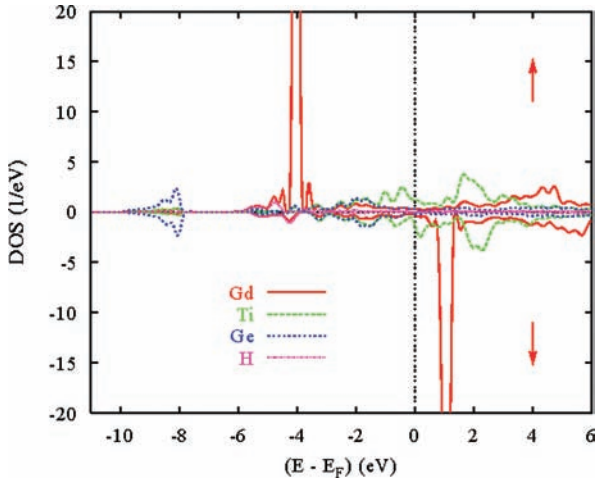

Figure 9. SP DOS for GdTiGeH in all-electron calculations.

Table 4. Interatomic Distances (Å) in the Structures of GdTiGe and GdTiGeH

		GdTiGe[28]	GdTiGeH
Gd	4 Ge	2.992(3)	3.036(4)
	1 Ge	3.154(11)	3.435(2)
	4 Ti	3.384(4)	3.555(2)
	4 Gd	3.700(5)	3.634(3)
	4 Gd	4.067(3)	3.981(8)
Ti:	4 Ge	2.768(5)	2.689(3)
	4 Ti	2.876(1)	2.815(4)
	4 Gd	3.384(4)	3.555(2)
Ge:	4 Ti	2.768(5)	2.689(3)
	4 Gd	2.992(3)	3.036(4)
	1 Gd	3.154(11)	3.435(2)
	1 Ge	3.757(9)	3.617(2)

latter two are weakened. This is likely connected with the distance magnitudes (see the Discussion above on structural changes induced by hydrogenation) and indicates large changes of the structure upon hydrogen uptake as it can be inferred from Figure 1.

Interestingly, bonding with hydrogen is most significant for Gd−H and Ge−H (for available diffuse like Ge p states), while Ti−H is found to be smallest. Gd−H bonding is likely to destroy the ferromagnetic ordering, leading to a paramagnetic ground state for GdTiGeH.

B. All-Electron Spin-Polarized Calculations. As may be expected from the large presence of the Gd 4f PDOS at E_F, the moment of Gd is ~7 μ_B in both compounds: (i) for GdTiGe μ_{Gd} = 7.28 μ_B, μ_{Ti} = 0.77 μ_B, μ_{Ge} = 0.02 μ_B, and μ_{cell} = 16.3 μ_B and (ii) for GdTiGeH μ_{Gd} = 7.01 μ_B, μ_{Ti} = 0.54 μ_B, μ_{Ge} = −0.01 μ_B, and μ_{cell} = 15.1. This is illustrated in Figure 9, showing the spin- and site-projected density of states for the hydrogenated compound. The positions of the Gd 4f states are very similar to the results obtained for GdTiGe by Skorek et al.,[40] who admitted not correctly finding the energy position of Gd 4f states in their calculations. This is also our problem here.

C. Using the PAW Methodology. In the presence of such shortcomings of the all-electron approach, we used the PAW methodology to have a better approach to experiment.[32]

Table 5. Experimental and Calculated Lattice Parameters[a]

	GdTiGe exp./calcd	GdTiGeH exp./calcd
a (Å)	4.067/4.047	3.981/3.959
c (Å)	15.475/15.524	16.377/16.50
vol. (Å^3)	255.96/254.26	259.57/258.8
Gd (4*e*)	(0, 0, 0.331)/(0, 0, 0.327)	(0, 0, 0.320)/(0, 0, 0.321)
Ti (4*c*)	(0, 1/2, 0)/idem	(0, 1/2, 0)/idem
Ge (4*e*)	(0, 0, 0.140)/(0, 0, 0.12)	(0, 0, 0.1104)/ (0, 0, 0.110)
H (4*d*)		(0, 1/2, 1/4)/idem
d_{Gd-H} (Å)		2.30

[a] Wyckoff positions refer to the space group *I*4/*mmm*.

Projector-augmented wave potentials are generated for use in different computational methods; they are transferable based on plane waves and pseudopotentials, such as the VASP method we use here (as well as Quantum Espresso, Abinit, Siesta, etc.). In the present work we use PAW-GGA VASP calculations to account for open-core Gd 4f states (found at ca. −17.5 eV) in the total DOS plot here below. The spin degenerate NSP as well as the SP calculations are done for both GdTiGe and its hydride. The latter assuming different hypotheses of the H position.

The calculations start from the experimental crystal data which are optimized. The results show little deviation with respect to the values in Table 3 as shown in Table 5 beside the experimental input values. The energy for GdTiGe is E = −37.503 eV. When H is introduced at the 4*d* position, i.e., within [Gd_4] tetrahedra (Table 5), the optimization gives as interatomic distance Gd−H = 2.30 Å in good agreement with experiment. The total energy is then E = −46.113 eV. If one out of the two H is removed, the energy for $GdTiGeH_{0.50}$ is then −41.788 eV. Then the energy difference per H is −4.61 eV. This is done in order to compare with three other possibilities for H positions in $GdTiGeH_{0.50}$, namely, at (0, 0, 0), (0, 0, 1/2), and (1/2, 1/2, 1/2). The total energies are then −40.669, −40.705, and −40.706 eV, respectively, yielding −3.17 and −3.20 eV per H, i.e., all less favorable than the H@4d hypothesis. The Gd−H distance is then shorter: 1.82 Å. Lastly, we checked the hypothesis of $GdTiGeH_4$ with 8 H at the 16*n* position (1/2 3/4 z~0.30). The resulting energy of E = −61.404 eV gives −2.98 eV per H. This is also unfavorable versus the H@4*d* hypothesis.

C.1. Equation of State EOS. Subsequent spin-polarized calculations were done with full geometry optimization.

Little changes versus the atomic positions calculated above (Table 5) were found and a better agreement with a slight increase of the unit cell volume for GdTiGe. For this ternary germanide, a magnetization of 2.68 μ_B was found while no magnetization could be identified for the hydride. The results are gathered in Figure 10 of the spin-polarized equation of state EOS for GdTiGe and the equilibrium values: the volume is very close to experiment (2 × 128.52 = 257.04 Å^3 versus 255.96 Å^3); the slightly larger calculated value is due to the use of the GGA functional which is *underbinding*, i.e., versus the LDA which is *overbinding*. For the importance of examining the magnetovolume effects, the variation of the magnetization is given together with the EOS. It can be seen that the magnetization changes significantly with volume, indicating the itinerant (delocalized) role of the electrons in the magnetism.

C.2. Density of States DOS. In Figures 11 and 12 we show the total spin-projected density of states for an illustration of the results for both GdTiGe and GdTiGeH, respectively. In both panels the low-energy lying Gd 4f states are found at ca. −17 eV.

dx.doi.org/10.1021/ic201579r |*Inorg. Chem.* 2011, 50, 11046–11054

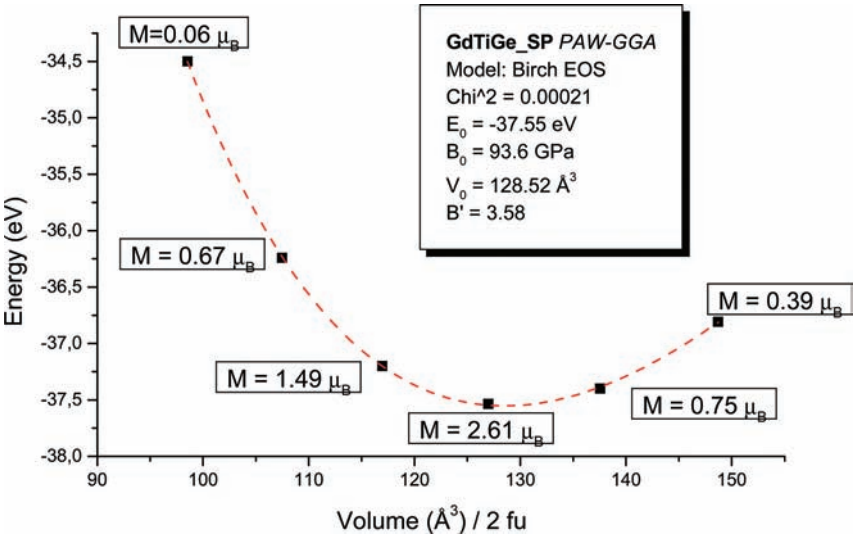

Figure 10. GdTiGe energy versus volume curve fitted with Birch EOS with fit values and relevant magnetizations.

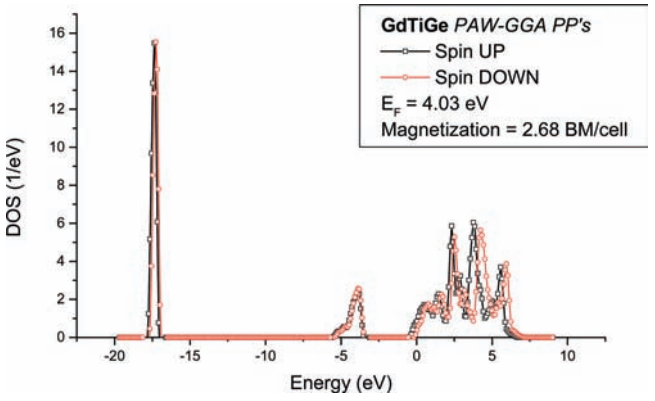

Figure 11. GdTiGe spin-projected total DOS from PAW-GGA calculations. Notice the energy position of Gd 4f states at ∼−17 eV.

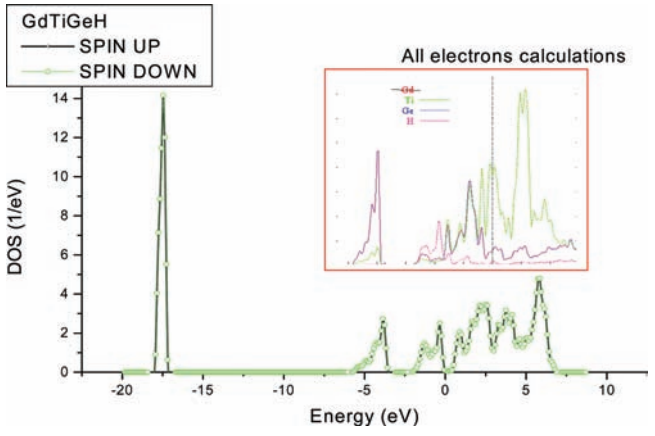

Figure 12. GdTiGeH spin-projected total DOS from PAW-GGA calculations. (Insert) PDOS from the all-electron calculations exhibiting the agreement for general shape and relative energy positions of the peaks.

The GdTiGe DOS (Figure 11) shows an energy shift between spin UP (↑) to lower energies versus spin DOWN (↓) DOS due to magnetic exchange, giving rise to a finite magnetization of 2.68 μ_B. On the contrary, there is no such energy shift in GdTiGeH as shown in Figure 12. The insert shows the corresponding NSP DOS obtained by the all-electron method (cf. Figure 7), showing large similarities except for the Gd 4f states not shown here.

C.3. Charges Analyses. Then it becomes interesting to examine the relative change of the occupation of the itinerant states on Gd between GdTiGe and its hydride: (i) GdTiGe Gd 6s (0.423), 6p (0.533), and 5d (1.182) and (ii) GdTiGeH Gd 6s (0.32), 6p (0.447), and 5d (1.090). In the hydride, there is a decrease of the number of electrons at the Fermi level due to insertion of hydrogen, affecting essentially the itinerant states. A Bader charge analysis on hydrogen shows that its charge amounts to ca. −0.6. This implies covalently bonded hydrogen, i.e., much more than in an ionic hydride such as MgH_2 where the charge is H^{-1}.

CONCLUSION

Hydrogenation of the ferromagnetic compound GdTiGe (CeScSi type) induces a drastic change in its magnetic properties. Indeed, the hydrogenated compound GdTiGeH is paramagnetic in the temperature range 4−300 K. The same hydride was obtained through hydrogenation of the CeFeSi-type modification which is antiferromagnetic below 412 K. Hydrogenation of the pristine compound induces a small increase of the compactness of the layers [Gd_4] and TiGe and a significant increase of their separation from one to each other along the *c* axis. From first-principles calculations it was found that the PAW GGA methodology is most adapted to treat Gd 4f states and reproduce the experimental observation for the magnetic orders of GdTiGe (ferromagnetic) and its hydride which presents no long-range magnetic order as well as to provide energetic bases for the position of H at the 4d site. From the computed significant change of magnetization with volume the itinerant electrons (not localized f like ones) are found to play a major role in GdTiGe. The chemical bonding shows that if the Gd−H bond is dominant then Ge−H is due to the s,p character of Ge states, while the Ti−H interaction is weakest.

AUTHOR INFORMATION

Corresponding Author

*E-mail: gaudin@icmcb-bordeaux.cnrs.fr.

■ ACKNOWLEDGMENT

Computations were carried out on the mainframe supercomputers of the M3PEC-Mésocentre, belonging to the University Bordeaux 1 and partly financed by the Conseil Régional d'Aquitaine and the French Ministry of research and technology (MRNT). This work was supported by the Deutsche Forschungsgemeinschaft through SPP 1458 *Hochtemperatursupraleitung in Eisenpnictiden*. Discussions with Dr. Volker Eyert from Materials Design Co. are gratefully acknowledged.

■ REFERENCES

(1) Kamihara, Y.; Hiramatsu, H.; Hirano, M.; Kawamura, R.; Yanagi, H.; Kamiya, T.; Hosono, H. *J. Am. Chem. Soc.* **2006**, *128*, 10012.
(2) Kamihara, Y.; Watanabe, T.; Hirano, M.; Hosono, H. *J. Am. Chem. Soc.* **2008**, *130*, 3296.
(3) Pöttgen, R.; Johrendt, D. *Z. Naturforsch.* **2008**, *63*, 1135.
(4) Chevalier, B.; Gaudin, E.; Weill, F.; Bobet, J.-L. *Intermetallics* **2004**, *12*, 437.
(5) Chevalier, B.; Pasturel, M.; Bobet, J.-L.; Isnard, O. *Solid State Commun.* **2005**, *134*, 529.
(6) Chevalier, B.; Gaudin, E.; Tencé, S.; Malaman, B.; Fernandez, J. R.; André, G.; Coqblin, B. *Phys. Rev. B* **2008**, *77*, 014414.
(7) Chevalier, B.; Tencé, S.; Gaudin, E.; Matar, S. F.; Bobet, J.-L. *J. Alloys Compd.* **2009**, *480*, 43.
(8) Tencé, S.; Matar, S. F.; André, G.; Gaudin, E.; Chevalier, B. *Inorg. Chem.* **2010**, *49*, 4836.
(9) Mizoguchi, H.; Hosono, H. *Chem. Commun* **2011**, *47*, 3778.
(10) Villars, P.; Calvert, L. D. *Pearsońs Handbook of Crystallographic Data for Intermetallic Phases*, 2nd ed.; American Society for Metals: Materials Park, OH, 1991; desk edition, 1997.
(11) Morozkin, A. V.; Seropegin, Yu. D.; Portnoy, V. K.; Leonov, A. V.; Sviridov, I. A. *J. Alloys Compd.* **1998**, *278*, 1.
(12) Bodak, O. I.; Kokhan, Z. M. *Inorg. Mater.* **1983**, *19*, 987.
(13) Chevalier, B.; Hermes, W.; Gaudin, E.; Pöttgen, R. *J. Phys.: Condens. Matter* **2010**, *22*, 146003.
(14) Morozkin, A. V.; Viting, L. M.; Sviridov, A.; Tskhadadze, I. A. *J. Alloys Compd.* **2000**, *297*, 168.
(15) Morozkin, A. V.; Seropegin, Yu. D.; Sviridov, I. A.; Moskalev, V. A. *J. Alloys Compd.* **1998**, *281*, 228.
(16) Morozkin, A. V.; Sviridov, I. A. *J. Alloys Compd.* **2001**, *320*, L1.
(17) Manfrinetti, P.; Provino, A.; Gschneidner, K. A., Jr. *J. Alloys Compd.* **2009**, *482*, 81.
(18) Lemoine, P.; Vernière, A.; Marêché, J. F.; Malaman, B. *J. Alloys Compd.* **2010**, *508*, 9.
(19) Chevalier, B.; Hermes, W.; Heying, B.; Rodewald, U. Ch.; Hammerschmidt, A.; Matar, S. F.; Gaudin, E.; Pöttgen, R. *Chem. Mater.* **2010**, *22*, 5013.
(20) Nikitin, S. A.; Tskhadadze, I. A.; Telegina, I. V.; Morozkin, A. V.; Seropegin, Y. D. *J. Magn. Magn. Mater.* **1998**, *182*, 375.
(21) Gaudin, E.; Tencé, S.; Weill, F.; Fernandez, J. R.; Chevalier, B. *Chem. Mater.* **2008**, *20*, 2972.
(22) Brück, E. *J. Magn. Magn. Mater.* **2007**, *310*, 2793.
(23) Chen, Y. F.; Wang, F.; Shen, B. G.; Hu, F. X.; Sun, J. R.; Wang, G. J.; Cheng, Z. H. *J. Phys.: Condens. Matter* **2003**, *15*, L161.
(24) Fujita, A.; Fujieda, S.; Hasegawa, Y.; Fukamichi, K. *Phys. Rev. B* **2003**, *67*, 104416.
(25) Tskhadadze, I. A.; Chernyshev, V. V.; Streletskii, A. N; Portnoy, V. K.; Leonov, A. V.; Sviridov, I. A.; Telegina, I. V.; Verbetskii, V. N.; Seropegin, Y. D.; Morozkin, A. V. *Mater. Res. Bull.* **1999**, *34*, 1773.
(26) Bobet, J.-L.; Pechev, S.; Chevalier, B.; Darriet, B. *J. Alloys Compd.* **1998**, *267*, 136.
(27) Petricek, V.; Dusek, M.; Palatinus, L. *Jana2006, The Crystallographic Computing System*; Institute of Physics: Praha, Czech Republic, 2006
(28) Welter, R.; Morozkin, A. V.; Klosek, V.; Vernière, A.; Malaman, B. *J. Alloys Compd.* **2000**, *307*, 207.
(29) Hohenberg, P.; Kohn, W. *Phys. Rev.* **1964**, *136*, B864.
(30) Kohn, W.; Sham, L. J. *Phys. Rev.* **1965**, *140*, A1133.
(31) Kresse, G.; Furthmüller, J. *Phys. Rev. B* **1996**, *54*, 11169.
(32) Kresse, G.; Joubert, J. *Phys. Rev. B* **1999**, *59*, 1758.
(33) Blöchl, P. E. *Phys. Rev. B* **1994**, *50*, 17953.
(34) Perdew, J. P.; Burke, K.; Ernzerhof, M. *Phys. Rev. Lett.* **1996**, *77*, 3865.
(35) Eyert, V. The Augmented Spherical Wave Method-A Comprehensive Treatment. In *Lecture Notes in Physics*; Springer: Berlin, Heidelberg, Germany, 2007; Vol. 719.
(36) Eyert, V. *J. Comput. Phys.* **1996**, *124*, 271.
(37) Hoffmann, R. *Angew. Chem., Int. Ed. Engl.* **1987**, *26*, 846.
(38) Morozkin, A. V.; Seropegin, Yu. D.; Sviridov, I. A. *J. Alloys Compd.* **1999**, *285*, L5.
(39) Ellner, M.; Reule, H.; Mittemeijer, E. J. *J. Alloys Compd.* **1998**, *279*, 179.
(40) Skorek, G.; Deniszczyk, J.; Szade, J.; Szade, J.; Tyszka, B. *J. Phys.: Condens. Matter* **2001**, *13*, 6397.